Catal Lett (2007) 118:91–97
DOI 10.1007/s10562-007-9155-0

Water–Gas Shift Reaction Over Aluminum Promoted Cu/CeO_2 Nanocatalysts Characterized by XRD, BET, TPR and Cyclic Voltammetry (CV)

Lei Li · Yingying Zhan · Qi Zheng · Yuanhui Zheng · Xingyi Lin · Dalin Li · Junjiang Zhu

Received: 15 May 2007 / Accepted: 10 June 2007 / Published online: 26 June 2007

Abstract A series of aluminum promoted Cu/CeO_2 nanocatalysts with aluminum content in the range of 0–5wt.% were prepared by co-precipitation method and examined with respect to their catalytic performance for the water–gas shift (WGS) reaction. The catalysts were characterized by XRD, BET, H_2-TPR and cyclic voltammetry (CV) techniques. The results indicate that catalytic activity increases with the aluminum content at first, but then decreases with the further increase of aluminum content. Hereinto, Cu/CeO_2 catalyst doped with 1 wt.% of aluminum shows the highest catalytic activity (CO conversion reaches 84.4% at 200 °C) and thermal stability for WGS reaction. Correlation to the results from above characterization, it is found that the variation of catalytic activity is in very agreement with that of the surface area, the area of peak γ (i.e., the reduction of surface copper oxide (crystalline forms) interacted with surface oxygen vacancies on ceria), and the area of peak C_2 and $A_1(Cu^0 \leftrightarrow Cu^{2+}$ in cyclic voltammetry process), respectively. Enough evidence was found for the fact that the metallic copper (Cu^0) interacted with surface oxygen vacancies on ceria is the active site for WGS reaction over Cu/CeO_2 catalysts.

Keywords Cu/CeO_2 catalyst · Water–gas shift · Aluminum · Active site · Cyclic voltammetry (CV)

L. Li · Y. Zhan · Q. Zheng (✉) · Y. Zheng · X. Lin · D. Li · J. Zhu
National Engineering Research Center of Chemical Fertilizer Catalysts, Fuzhou University, Gongye Road 523, Fuzhou 350002, P.R. China
e-mail: qizheng2005@gmail.com

1 Introduction

The water–gas shift (WGS) reaction, $CO + H_2O \leftrightarrow CO_2 + H_2$, was used industrially for the production of hydrogen in synthesis of ammonia and adjusting the CO/H_2 ratio for subsequent synthesis of methanol. In recent years, the WGS reaction has become an interesting field again because of its essential role in supplying hydrogen for fuel-cell power generation [1], in which the traditional WGS catalysts are unsuitable due to the harsh reaction conditions [2]. Thus, there is a critical requirement for new and more effective catalysts for WGS reaction. It has been reported that the supported precious metal catalysts, such as Au/CeO_2 [3], Au/TiO_2 [4], Au/Fe_2O_3 [5], Pd/CeO_2 [6], Pt/TiO_2 [7], Pt/CeO_2 [8], Rh/Fe_2O_3 [9] and so on, showed high catalytic activity for the reaction. However, considering the high cost of the above precious metals or their instability, more and more attention has been focused on the base metal catalysts including copper.

Many studies [10–13] have shown that ceria-supported copper catalysts exhibit highly activity for the WGS reaction. Li et al. [10] recently reported that Cu-loaded ceria catalyst (especially 5% Cu–Ce (La) O_x) retained highly catalytic activity for the WGS reaction even at 600 °C, with the feed gas only containing CO, H_2O and inert gas. In order to apply these catalysts in fuel-cell power generation, Qi et al. [12] investigated the effect of H_2 and CO_2 on the activity and stability of $Cu–CeO_2$ catalysts for the reaction, finding that both activity and stability of such catalysts decreased when H_2 and CO_2 being added. Therefore, it is a challenge work to find out a suitable catalyst for WGS reaction at the presence of H_2 and CO_2.

To the best of our knowledge, few attempts have been made to promote or stabilize Cu/CeO_2 catalysts. Andreeva et al. [14] reported that the addition of aluminum could

improve the stability of Au/CeO_2 catalysts for WGS reaction. Yahiro et al. [15] reported a highly catalytic activity of copper supported on γ-aluminum for WGS reaction. And several CeO_2-doped CuO/γ-Al_2O_3 catalysts, which were prepared by wet impregnation method, were evaluated for the CO oxidation [16], steam reforming of methanol [17], NO+CO reaction [18] and so on. Whereas, no work regarding the catalysts of copper oxide supported aluminum-promoted ceria (prepared by co-precipitation) for WGS reaction has been reported.

In this present work, aluminum was introduced to Cu/CeO_2 catalyst, with a co-precipitation method, to modify its activity and stability. The results suggest that only small doping (ca. 1 wt.%) of aluminum can increase the number of active site (i.e., the metallic copper interacted with surface oxygen vacancies on ceria) for WGS reaction and subsequently show the highest catalytic performance. The correlation of catalyst structure and catalytic performance was investigated by XRD, BET, H_2-TPR and CV techniques. Especially, cyclic voltammetry (CV) was applied, for the first time, to character the active site of the WGS reaction over Cu/CeO_2 catalysts and furnish enough information for correlating catalytic activity.

2 Experimental

2.1 Preparation of Catalysts

A series of aluminum doped Cu/CeO_2 catalysts with fixed Cu content (30 wt.%, calculated as CuO) and a given aluminum content (e.g., 0, 1, 3, 5 wt.%, calculated as Al_2O_3) were prepared by parallel co-precipitation method. The obtained samples were denoted as CCA0, CCA1, CCA3 and CCA5, respectively. Stoichiometric amounts of $Cu(NO_3)_2 \cdot 3H_2O$, $Ce(NO_3)_3 \cdot 6H_2O$ and $Al(NO_3)_3 \cdot 9H_2O$ were first dissolved in deionized water, then the mixed aqueous solution were co-precipitated with an aqueous solution of KOH, with vigorous stirring at T = 80 °C and PH = 10 ± 1. A black suspension was acquired and aged with continuous stirring at 80 °C for 6 h. The resulting precipitate was centrifuged and washed by deionized water for several times, then dried at 120 °C for 12 h and finally calcined at 650 °C for 4 h (heating rate was 5 °C/min) in air.

2.2 Characterizations of Catalysts

Power XRD patterns of the as-synthesized samples were recorded by a PANalytical X' pert Pro diffractometer equipped with Cu–Kα (λ = 0.1541 nm) radiation operating at 40 kV and 40 mA for 2θ angles ranging from 25 to 75°. The crystal size of ceria and copper oxide was determined from the peak broadening by the Scherrer equation.

The BET surface area and pore volume were measured on an NOVA 4200e instrument, at –196 °C using nitrogen as adsorption gas. Prior to each analysis, the sample was degassed at 250 °C for 3 h to obtain a residual pressure of less than 10^{-5} Torr.

Temperature-programmed reduction (TPR) measurement was carried out on an AutoChem 2910 instrument. The H_2-TPR was performed by passing 10% H_2/Ar (flowing rate = 30 mL/min) on 50 mg catalyst at a heating rate of 10 °C/min. Prior to TPR, the samples were pretreated under a 10% O_2/Ar mixture at 400 °C for 30 min. Then the system was cooled to ambient temperature under a pure Argon gas. The hydrogen consumption was monitored using a thermal conductivity detector (TCD).

The cyclic voltammetry (CV) spectra were recorded at ambient temperature using a CHI 611B potentiostat/galvanostat with three-electrode cell configuration. About 10 mg of catalysts and 2 mg of carbon black (Vulcan XC-72R) were suspended in 2 ml of ethanol and 30 μL of Nafion solution to prepare catalyst ink. Then 25 μL of ink was transferred with an injector to clean glassy carbon disk electrode. After the ethanol volatilization, the electrode was heated at 75 °C for 5 min. Sodium sulfate (0.05 M) was used as the electrolyte solution. The counter and reference electrodes are Pt foil and $Hg/Hg_2SO_4/H_2SO_4$ (0.5 M), respectively. Prior to the measurement, the electrolyte solution was degassed by bubbling with high pure nitrogen (99.999%). The electrodes were cycled from +0.8 to –1.6 V at a scan rate of 10 mVs^{-1}.

2.3 Evaluation of Catalytic Performance

The catalytic activities and thermal stabilities of the catalysts for WGS reaction were tested in a fixed bed reactor at atmospheric pressure. About 3 g of catalysts (20–40 mesh) was placed between two layers of quartz granules inside a stainless steel tube (i.d. = 12 mm). The experiment was directly performed under a feed gas (25% CO, 50% H_2, 8% CO_2 and balance N_2) flowing at 100 mL/min without pre-reduction. The ratio of vapor to feed gas was maintained at 1:1. The residual water of the outlet was removed by a condenser before entering a gaschromatograh (102G) equipped with a thermal conductivity detector (TCD). The activity was expressed by the conversion of CO, defined as: $X_{CO}(\%) = (1 - V'_{CO}/V_{CO}) \times 100\%/(1 + V'_{CO})$, where V_{CO} and V'_{CO} are the inlet and outlet content of CO, respectively. The catalytic activity was first measured from 200 to 400 °C, then kept at 400 °C for 10 h and decreased to 180 °C, and finally increased to 300 °C to investigate the thermal stability of the catalysts.

3 Results and Discussion

3.1 Activity and Stability of Catalysts

Figure 1 depicts the WGS activities of the aluminum doped Cu/CeO_2 catalysts. The CO conversion increased with the aluminum content at first (from CCA0 to CCA1), but then decreased with the further increase of aluminum content. The CO conversion reached the maximum at CCA1, with the value of 84.4% at 200 °C, which is an increase of 11.8% comparing with that of CCA0 (75.5%).

Figure 2 shows the thermal stabilities of aluminum doped Cu/CeO_2 catalysts at 300 °C for WGS reaction. As seen in Fig. 2a the CO conversion of CCA1 decreased from 90.2% to 86.5%, corresponding to the relative deactivation of 4.1%, which is smaller than that of CCA0, CCA3 and CCA5. It was observed from Fig. 2b that all the catalysts deactivated slightly, but the present aluminum doping can enhance thermal stability of CuO/CeO_2 catalysts for WGS reaction to some extent. Above all, CCA1 shows the highest thermal stability among the catalysts.

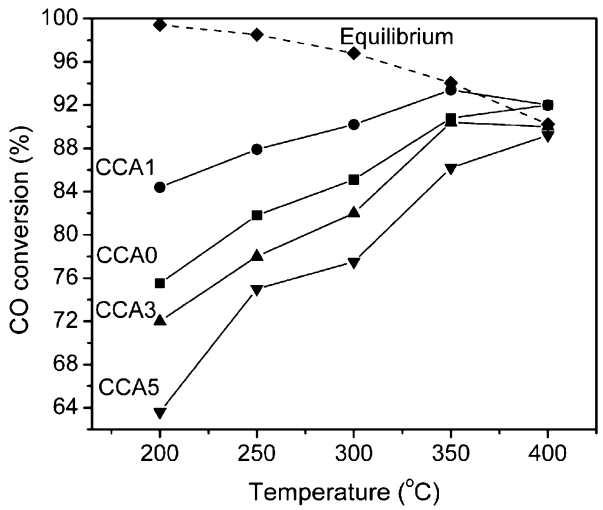

Fig. 1 WGS activities of the aluminum doped Cu/CeO_2 catalysts. Feed gas: 25% CO, 50% H_2, 8% CO_2 and balance N_2; Vapor–gas: 1:1 (mol); W/F = 1.8 g s cm^{-3}

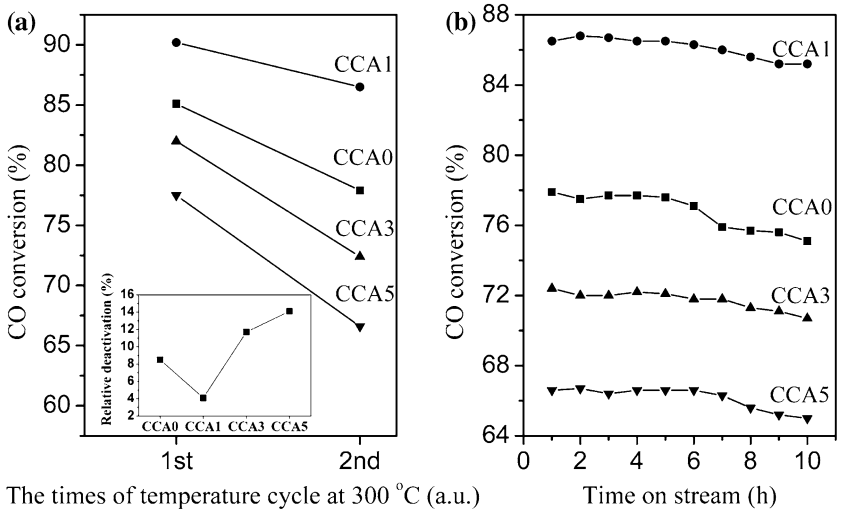

Fig. 2 Thermal stabilities of aluminum doped Cu/CeO_2 catalysts after the first evaluation. (**a**) Comparison between the first and second initial activity at 300 °C (inset: Relative deactivation of the catalysts at 300 °C). (**b**) CO conversion vs. time on stream at 300 °C. *Note:* After the first evaluation, the samples were successively exposed to the feed gas at the given temperature procedure (Keep at 400 °C for 10 h and then down to 180 °C, and finally ramp to 300 °C)

3.2 Catalysts Characterizations

3.2.1 XRD Study of the As-Synthesized Catalysts

Figure 3 is the XRD patterns of the prepared samples. The distinct fluorite oxide diffraction pattern of CeO_2 and the strong diffraction peaks of CuO were detected in all of the samples. No obvious diffraction lines, ascribed to aluminum or alumina, were detected, which indicates that aluminum might entered the CeO_2 frame or alumina was highly dispersed in the catalysts. With the increase of aluminum content, the cell parameter of CeO_2 (111) is

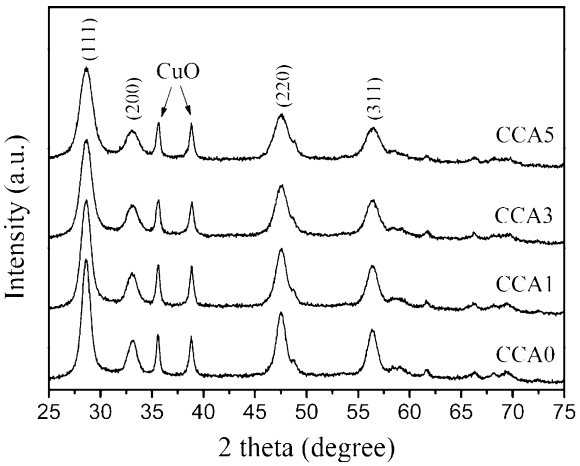

Fig. 3 XRD patterns of as-synthesized aluminum doped Cu/CeO_2 catalysts

Table 1 Physical properties of the as-synthesized catalysts

Catalysts	$S_{BET}(m^2/g)$		Pore volume (ml/g)	Crystal size (nm)[b]		Cell parameter (nm)[c]	Lattice strain (%)[d]	
	Fresh	Used[a]		CeO_2(111)	CuO(111)	a_{CeO_2}	CeO_2(111)	CuO(111)
CCA0	53	39	0.15	8.8	26.1	0.5405	1.566	0.413
CCA1	64	50	0.15	7.1	19.8	0.5403	1.678	0.473
CCA3	50	35	0.11	6.2	19.3	0.5399	1.922	0.489
CCA5	44	29	0.10	5.7	20.9	0.5398	2.211	0.483

[a] The catalysts undergone the activities and thermal stabilities test and were cooled to ambient temperature without feed gas

[b] Calculated from the peak at 28.6°, 35.6° for CeO_2 (111), CuO (111) by the Scherrer equation, respectively

[c] Calculated from the peak at 28.6° by $d^2 = a^2/(H^2 + K^2 + L^2)$ equation depended on d-spacing

[d] Calculated from the peak at 28.6°, 35.6° for CeO_2 (111), CuO (111), respectively

almost identical, indicating that the doping alumina was highly dispersed in the catalysts rather than entered the CeO_2 frame, because of the small ion radius of aluminum ($r_{Al}^{3+} = 0.054$nm, $r_{Ce}^{4+} = 0.092$ nm). As the doping concentration of aluminum increases, the crystal size of CeO_2 (111) decreased gradually (from 8.8 nm to 5.7 nm, see Table 1), corresponding to the attenuating and broadening of diffraction peaks of CeO_2. Moreover, the crystal size of CuO in CCA1, CCA3 and CCA5 are close to each other and lower than that in CCA0 sample.

Xie et al. [19] reported the spontaneous monolayer dispersion principle that many oxides and salts can disperse spontaneously onto the surface of supports to form a monolayer or submonolayer. Chen et al. [20] calculated the dispersion threshold of many oxides and salts on the supports by the "Incorporation Model". The results indicate that the dispersion threshold of alumina on the ceria is 0.0622 g/100 m^2. Similarly, the dispersion threshold of alumina on the as-synthesized catalysts is about 0.016 g/1 g (i.e., 1.6 wt.%). The reason for the decrease of the crystal size might be ascribed to that the doping alumina, dispersed spontaneously onto the surface of the supports to form the monolayer or submonolayer, prevented the agglomeration of copper oxide and ceria. On the other hand, the lattice strain of CeO_2 (111) increased obviously with the increase of aluminum content, while the variation of lattice strain of CuO is minor and could be neglected, indicating that the doping alumina has larger effect on the CeO_2 than the CuO. This suggests that the alumina disperses primarily onto the surface of CeO_2 rather than that of CuO.

3.2.2 *Texture of Catalysts*

The texture properties of the catalysts are listed in Table 1. BET surface area of fresh catalysts varied with the aluminum content, and reached the maximum at CCA1 (64 m^2/g), which is an increase of 21% comparing with that of CCA0 (53 m^2/g). The largest surface area of CCA1 might be attributed to that the appropriate amount (smaller than the dispersion threshold) of alumina, dispersed spontaneously onto the surface of CeO_2, prevented the agglomeration of copper oxide and ceria. While the decreasing surface area of CCA3 and CCA5 are probably due to that the excess alumina continued dispersing spontaneously onto the surface of CuO to form a copper aluminate surface phase and even form a few spinel species (e.g. $CuAl_2O_4$) [21], which was also dispersed spontaneously to form the monolayer. It is found that the variation of surface area has the same trend as that of catalytic activity, indicating that the surface area has large effect on the catalytic performance in the present case. Besides, the surface area of used catalysts is smaller than that of the fresh ones (e.g., 22% for CCA1), which suggests the increase of particle size during the activity evaluation leads to the deactivation of the catalysts.

3.2.3 *H_2-TPR*

Figure 4 is the H_2-TPR profiles of the samples. All the curves are fitted into four peaks by Gauss–Lorentz method as that in [22]. The peak positions and their contributions are summarized in Table 2. According to literatures [23–25], the peak α and peak β are attributed to the reduction of non-crystalline copper oxide strongly interacting with CeO_2 and that of larger copper oxide particles weakly associated with CeO_2, respectively. The peak γ is ascribed to the reduction of surface copper oxide (crystalline forms) which interacted with surface oxygen vacancies on ceria. The peak δ is due to the reduction of pure bulk crystalline copper oxide, which does not associate with CeO_2.

With the increase of aluminum content, the positions of all peaks increase gradually. Moreover, among all these peaks, the area of peak α and β is close to each other, while the area of peak γ reaches the maximum at CCA1 then decreases at CCA3 and CCA5 comparing with CCA0. As the aluminum content is smaller than the dispersion threshold (1.6 wt.%) of the alumina on the ceria, the doping

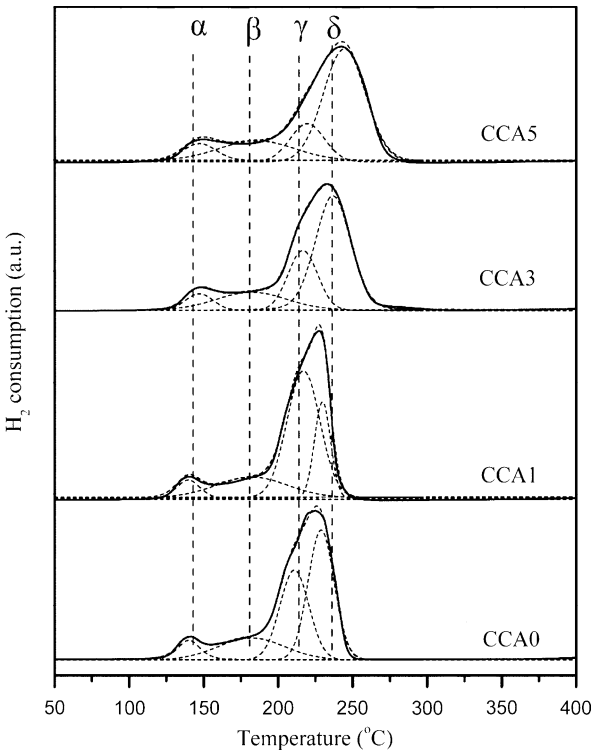

Fig. 4 H_2-TPR profiles of the aluminum doped Cu/CeO_2 catalysts. Solid lines are experimental curves and dot lines are Gauss–Lorentz fitted curves

alumina dispersed spontaneously onto the surface of CeO_2 to form the monolayer, prevented the agglomeration of copper oxide and ceria and improved the mutual dispersion degree between the crystal CuO and ceria, resulting in the increase of the crystal CuO interacted with the surface oxygen vacancies on ceria. Thus the area of peak γ reaches the maximum at CCA1. While the decreasing area of peak γ at CCA3 and CCA5 might be attributed to that the excess alumina continued dispersing spontaneously onto the surface of the crystal CuO and prevented the interaction between CuO and the surface oxygen vacancies on ceria. Correlation to the catalytic activities, it is obviously to find that the variation of peak γ' area is well consistent with that of catalytic activity, indicating that the area of peak γ has large effect on the catalytic activity. In other words, the catalytic activity might be mainly affected by the number of reducible surface copper oxide (crystalline forms) which interacted with surface oxygen vacancies on ceria.

3.2.4 *Cyclic Voltammetry*

The redox abilities of aluminum doped Cu/CeO_2 catalysts and their effects on the catalytic performances were also investigated with the aid of CV measurement, which was reported to be a powerful characteristic means in heterogeneous catalysis [26]. The cyclic voltammograms of copper species in aluminum doped Cu/CeO_2 catalysts are showed in Fig. 5. The voltammograms consist of two cathodic (peak C_1 and C_2) and two anodic (peak A_1 and A_2) peaks in the scan range of +0.8 to –1.6 V versus $Hg/Hg_2SO_4/H_2SO_4$ (0.5 M). In order to designate the peaks, the first step in the interpretation of cyclic voltammograms is the calculation of the thermodynamic, reversible potentials of all the possible reactions. The standard potential can be calculated as $E^\theta = -\Delta G^\theta/nF$. In the case of copper oxides, some possible reactions are:

$$2CuO + 2H^+ + 2e = Cu_2O + H_2O$$
$$E^\theta = 0.64V \text{ vs. SHE; at pH } 7, E_{rev} = 0.23V \text{ vs. SHE} \quad (1)$$

$$Cu_2O + 2H^+ + 2e = 2Cu + H_2O$$
$$E^\theta = 0.47 \text{ V vs. SHE; at pH } 7, E_{rev} = 0.06 \text{ V vs. SHE} \quad (2)$$

$$CuO + 2H^+ + 2e = Cu + H_2O$$
$$E^\theta = 0.56 \text{ V vs. SHE; at pH } 7, E_{rev} = 0.15 \text{ V vs. SHE} \quad (3)$$

where the E_{rev} is calculated as $E_{rev} = E^\theta + RT/nF \ln([Ox]/[Red])$ (Nernst's equation). In the case of the peak C_1 and C_2 of the CCA0 (Fig. 5a), the reversible potentials are about 0.30 V and 0.15 V vs. SHE, in very good agreement with the above Eq. 1 and 3. Actually, since a buffer was not

Table 2 H_2-TPR peak positions and concentrations of reducible species in aluminum doped Cu/CeO_2 catalysts as determined by the Gauss–Lorentz fit of TPR profiles

Catalysts	TPR peak position (temperature °C) and concentration (%)[a]			
	Peak α	Peak β	Peak γ	Peak δ
CCA0	140.1 (6.7)	182.1 (18.3)	210.9 (32.7)	228.8 (42.2)
CCA1	139.6 (6.6)	182.6 (18.0)	216.9 (51.3)	229.7 (24.1)
CCA3	147.0 (5.7)	182.3 (18.2)	216.5 (22.1)	236.8 (54.0)
CCA5	147.3 (7.3)	185.7 (18.2)	219.5 (16.1)	244.4 (58.4)

[a] Values in parentheses are the percent of each peaks area i.e. the contribution (%) of each species

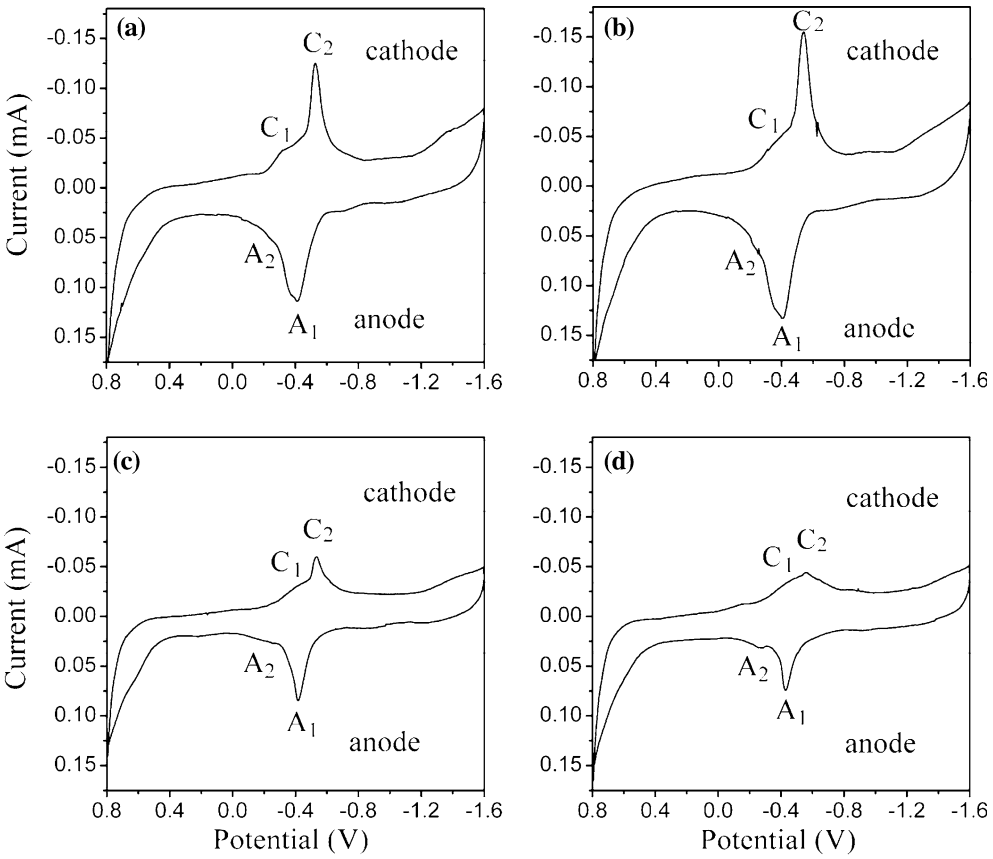

Fig. 5 Cyclic voltammograms of copper species in aluminum doped Cu/CeO_2 catalysts in 0.05 M Na_2SO_4 electrolyte at a scan rate of 10 mV s^{-1}. The counter and reference electrodes are Pt foil and $Hg/Hg_2SO_4/H_2SO_4$ (0.5 M), respectively. (**a**) CCA0; (**b**) CCA1; (**c**) CCA3; (**d**) CCA5

used, the approximate agreement is surprisingly good. Therefore, the peak C_1 is ascribed to the reduction of Cu^{2+} to Cu^{+}, and the peak C_2 is attributed to the reduction of Cu^{2+} to Cu^{0} (the sum of Cu^{2+} to Cu^{+} and Cu^{+} to Cu^{0}). Correspondingly, the peak A_1 is due to the oxidation of Cu^{0} to Cu^{2+}, and the peak A_2 is the oxidation of Cu^{+} to Cu^{2+}. In addition, the same CV measurement of pure CeO_2 (prepared as the same process) was also carried out, and there is no peak in the cyclic voltammograms (the result was not presented). Thus it is indicated that the Ce^{4+}/Ce^{3+} redox couple dose not exist in the potential range studied.

The area of peak $A_1(Cu^0 \rightarrow Cu^{2+})$, which represents the number of Cu^0 participating in the $Cu^0 \rightarrow Cu^{2+}$ reaction, reaches the maximum at CCA1 and then falls off at CCA3 and CCA5 comparing with CCA0. Particularly interesting is the finding that the variation of the peak area has the same trend as that of catalytic activity, indicating that the number of Cu^0 participating in the $Cu^0 \rightarrow Cu^{2+}$ reaction has large effect on the catalytic activity of WGS reaction in the present case.

On the other hand, the oxidative and reduction potentials for copper species in all cases are almost constant. Furthermore, Zhu et al. [26, 27] reported that ΔE of catalyst is not an intrinsic factor in deciding the catalytic activity when there exists a reducing agent in the feed gas. Similarly, we also consider that the ΔE of catalysts has less effect on the catalytic activity of WGS reaction, in which two reducing agents (CO and H_2) were existed. Accordingly, ΔE of catalysts will not be discussed in the present case.

3.2.5 Active Site of Cu/CeO_2 Catalysts for WGS Reaction

It is indicated above that the number of Cu^0 has large effect on the catalytic activity the WGS reaction. In order to further confirm the relation between the metallic copper and catalytic activity of WGS reaction, the tested sample (CCA1), which reacted with feed gas under the condition of WGS reaction at 200 °C for 3 h and then was protected from oxidation with benzene and polystyrene, was measured by X-ray power diffraction. The quasi situ XRD pattern of tested CCA1 is showed in Fig. 6. The distinct fluorite oxide diffraction pattern of CeO_2 and the strong diffraction peaks of Cu were detected, while the diffraction peaks of CuO disappeared and there was no diffraction peaks of suboxide (e.g., Cu_2O or Cu_4O_3), indicating that copper is present in the catalysts as metallic Cu under the condition of WGS reaction. Based on this, it is deduced that metallic copper (Cu^0) is the active site of WGS reaction carried out on Cu/CeO_2 catalysts. Combining with the

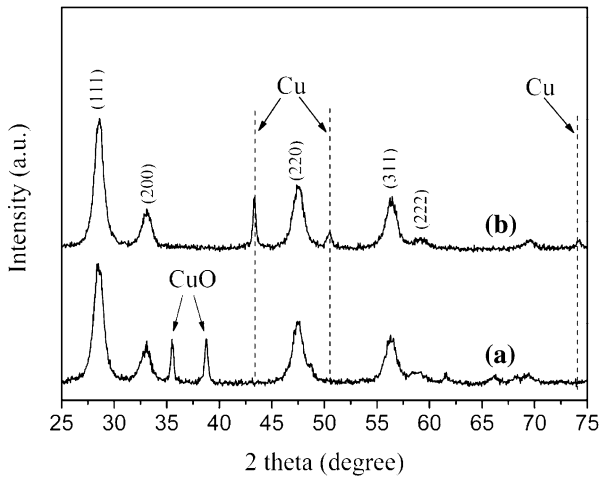

Fig. 6 XRD pattern of fresh CCA1 and tested CCA1. (**a**) fresh CCA1; (**b**) tested CCA1, which is the fresh CCA1 that reacted with feed gas under the condition of WGSR at 200 °C for 3 h and then was protected from oxidation with benzene and polystyrene

results from the H_2-TPR, CV and activity characterization, the metallic copper (Cu^0) should derive from the reduction of surface copper oxide (crystalline forms) interacted with surface oxygen vacancies on ceria, and hence, we concluded that it is the metallic copper (Cu^0) interacted with surface oxygen vacancies on ceria that plays a decisive role in the WGS reaction, which is very consistent with the results reported by Wang [28].

4 Conclusions

Cu/CeO_2 catalysts doped by aluminum (0, 1, 3, 5 wt.%) prepared by co-precipitation were evaluated for WGS reaction. The results indicate that as aluminum doping is 1 wt.%, the catalyst has the largest surface area and shows the highest catalytic activity and thermal stability. The area of the reductive peak γ (i.e., the reduction of surface copper oxide (crystalline forms) interacted with surface oxygen vacancies on ceria) and the peak C_2 and $A_1(Cu^0 \leftrightarrow Cu^{2+})$ reaches a maximum at CCA1, thus the highest catalytic activity of CCA1 can be ascribed to the most active sites. It is concluded that the metallic copper (Cu^0) interacted with surface oxygen vacancies on ceria plays a decisive role in the WGS reaction and is considered as the active site of the WGS reaction over Cu/CeO_2 catalysts.

Acknowledgment The authors gratefully acknowledge the financial support from the Department of Science of the People's Republic of China (20271012) and the Department of Science & Technology of Fujian Province (2005H201-2).

References

1. Trimm DL, Önsan ZI (2001) Catal Rev 43:31
2. Swartz SL, Seabaugh MM, Holt CT, Dawson WJ (2001) Fuel cells Bull 4:7
3. Fu Q, Weber A, Flytzani-Stephanopoulos M (2001) Catal Lett 77:87
4. Idakiev V, Yuan Z-Y, Tabakova T, Su B-L (2005) Appl Catal A 281:149
5. Zhang FL, Zheng Q, Wei KM, Lin XY, Zhang HH, Li JW, Cao YN (2006) Catal Lett 108:131
6. Wang X, Gorte RJ, Wagner JP (2002) J Catal 212:225
7. Panagiotopoulou P, Christodoulakis A, Kondarides DI, Boghosian S (2006) J Catal 240:114
8. Duarte de Farias AM, Barandas APMG, Perez RF, Fraga MA (2007) J Power Sources 165:854
9. Basinska A, Domka F (1997) Catal Lett 43:59
10. Li Y, Fu Q, Flytzani-Stephanopoulos M (2000) Appl Catal B 27:179
11. Liu W (1995) Sc.D. Thesis, Massachusetts Institute of Technology
12. Qi X, Flytzani-Stephanopoulos M (2004) Ind Eng Chem Res 43:3055
13. Pintar A, Batista J, Hočevar S (2007) J Colloid Interface Sci 307:145
14. Andreeva D, Ivanov I, Ilieva L, Abrashev MV (2006) Appl Catal A 302:127
15. Yahiro H, Nakaya K, Yamamoto T, Saiki K, Yamaura H (2006) Catal Commun 7:228
16. Park JW, Jeong JH, Yoon WL, Jung H, Lee HT, Lee DK, Park YK, Rhee YW (2004) Appl Catal A 274:25
17. Men Y, Gnaser H, Zapf R, Hessel V, Ziegler C, Kolb G (2004) Appl Catal A 277:83
18. Jiang XY, Lou LP, Chen YX, Zheng XM (2003) Mol J Catal A 197:193
19. Xie YC, Tang YQ (1990) Adv Catal 37:1
20. Chen Y, Zhang L (1992) Catal Lett 12:51
21. Larsson PO, Andersson A (2000) Appl Catal B 24:175
22. Yao CZ, Wang LC, Liu YM, Wu GS, Cao Y, Dai WL, He HY, Fan KN (2006) Appl Catal A 297:151
23. Zheng XC, Zhang XL, Wang XY, Wang SR, Wu SH (2005) Appl Catal A 295:142
24. Tang XL, Zhang BC, Li Y, Xu YD, Xin Q, Shen WJ (2004) Catal Today 93–95:191
25. George A, Theophilos I (2003) Appl Catal A 224:155
26. Zhu J, Zhao Z, Xiao D, Li J, Yang X, Wu Y (2005) Electrochem Commun 7:58
27. Zhu J, Zhao Z, Xiao D, Li J, Yang X, Wu Y (2005) J Mol Catal A 238:35
28. Wang X, Rodriguez JA, Hanson JC, Gamarra D, Arias AM, Garcia MF (2006) J Phys Chem B 110:428